In-Situ Heating Study on the Structural Change of Surfactant-Templated Germanium Oxide Mesostructure

Xing Chen,[†,‡] Quan Cai,[†,§] Wei Wang,[†,§] Guang Mo,[†,§] Longsheng Jiang,[†,§] Kunhao Zhang,[†,§] Zhongjun Chen,[†] Ziyu Wu,*[,†] and Zhonghua Wu*[,†]

Beijing Synchrotron Radiation Facility, Institute of High Energy Physics, Chinese Academy of Science, Beijing 100049, China, General Research Institute for Nonforrous Metals, Beijing 100088, China, and Graduate University of the Chinese Academy of Sciences, Beijing 100049, China

Received: April 18, 2008; Revised Manuscript Received: July 8, 2008

Mesostructured germanium oxide has been well-synthesized by using a surfactant-templated approach under basic hydrothermal conditions. The cationic surfactant cetyltrimethylammonium bromide (CTAB) has formed nanotubes with uniform diameter of about 3.2 nm. Blanket-like morphology of the as-prepared sample has been observed with transmission electron microscopy (TEM). High-resolution TEM image reveals that the nanotubes are connected with inorganic germanium oxide and have self-assembled into periodic mesostructure. In-situ heating X-ray diffraction (XRD) patterns confirm that the germanium oxide is in amorphous phase in the temperature range from room temperature (RT) to 700 °C. In-situ heating small-angle X-ray scattering (SAXS) presents the mesostructural change with temperature. The local atomic structures around germanium atom have been obtained with in-situ heating X-ray adsorption fine structure (XAFS) techniques. The stability of this mesostructure has been determined to be correlated with the cationic surfactant CTAB. The structural evolution from the GeO_2/NaOH aqueous solution, the as-prepared sample to the sample heated at 700 °C, has been described, and the formation mechanism of mesostructured germanium oxide has been discussed.

1. Introduction

Surfactant-templated mesoporous materials have stimulated wide interest since 1992 because of their potential applications in areas of catalysis, sorption, separation, and chemical sensing.[1−4] Although the most commonly studied mesoporous material is still silica, the current efforts are gradually extending to the synthesis of nonsiliceous oxide analogues due to their fascinating electronic, optical, magnetic, photochemical, and/or electrochemical behaviors. GeO_2, as a promising material, has been well-studied on its optical and electronic properties.[5−7] For example, one-dimensional GeO_2 nanowires were found to have good optical properties.[8] At the same time, GeO_2 nanocrystals were also attested to be blue photoluminescence materials with weak peak energies around 3.1 and 2.2 eV.[9,10]

As it is known, the electronic and optical properties of nanomaterials depend strongly on nanoparticle sizes, dimensionality, and structures. Assembling nanoparticles to some mesostructure is one of the methods to control and adjust the unique properties of nanomaterials. Usually, mesoscopic-structured germanium oxide was synthesized by using a surfactant-templated approach.[11] In this study, a mesostructured germanium oxide has been obtained, which exhibits blanket-like morphology with an amorphous inorganic wall. This germanium oxide mesostructure is different from the titanium, niobium, and tin oxide mesostructures.[12−15] The potential application of germanium oxide long-range-ordered mesostructure drives us to study its structural evolution. Despite the formation mechanism of organic−inorganic mesostructure materials having been well-studied,[16−19,11] the surfactant influence on mesoscopic and microscopic structures is still not very clear, especially the structural change of mesostructured germanium oxide with heating temperature. Here, in-situ heating X-ray diffraction (XRD), in-situ heating small-angle X-ray scattering (SAXS), and in-situ heating extended X-ray absorption fine structure (EXAFS) techniques are used to investigate the structural evolution of germanium oxide mesostructure.

2. Experimental Section

Preparation of Mesostructured GeO_2. Mesostructured germanium oxide was hydrothermally synthesized by using a similar surfactant-templated approach as in the literature.[11] In a typical synthesis procedure, 1.06 g of GeO_2 (5.0 mmol) and 1.54 mL of 2 M sodium hydroxide (NaOH) aqueous solution were added into 10 mL of distilled water to form solution A (marked as l-GeO_2), and 1.46 g of cetyltrimethylammonium bromide (CTAB) was dissolved into 12 mL of distilled water to form solution B. After the two solutions were stirred for 12 h at room temperature (RT), respectively, solution B was poured into solution A to form a mixture solution C. Then, the mixture C was stirred for 12 h at RT and moved into a Teflon bottle and kept at 100 °C for 56 h. The resulting product was washed with distilled water and absolute alcohol several times to remove impurities. Finally, the as-prepared power sample (marked as Ge025) was obtained by dying the product at RT.

TEM, XRD, SAXS, and XAFS Characterization. Ge025 was characterized by using a Hitachi H-600 TEM which was operated at 100 kV. In-situ heating XRD and SAXS patterns were recorded by using an imaging plate with X-ray wavelength of $\lambda = 1.54$ Å at beam line 4B9A of the Beijing Synchrotron Radiation Facility (BSRF).[20,21] In-situ heating X-ray-absorption fine-structure (XAFS) data of Ge K-edge were collected in transmission mode at the EXAFS station (beam line 1W1B) of

* To whom correspondence should be addressed. E-mail: wuzh@mail.ihep.ac.cn (Zhonghua Wu); wuzy@mail.ihep.ac.cn (Ziyu Wu).
† Institute of High Energy Physics, Chinese Academy of Science.
‡ General Research Institute for Nonforrous Metals.
§ Graduate University of the Chinese Academy of Sciences.

10.1021/jp803407a CCC: $40.75
Published on Web 09/06/2008

TABLE 1: Structural Parameters of Ge−O Bonds Obtained by Least-Squares Fitting the Experimental EXAFS Data[a]

sample	bonds	N	R (Å)	σ^2 (Å^2, $\times 10^{-3}$)	ΔE (eV)	$\sigma^{(3)}$ (Å^3, $\times 10^{-4}$)
l-GeO_2	Ge−O	4.1 ± 0.4	1.79 ± 0.01	5.9 ± 2.1	3.5 ± 0.5	2.4 ± 0.4
Ge025	Ge−O	4.1 ± 0.3	1.78 ± 0.01	6.2 ± 2.3	3.6 ± 0.5	2.8 ± 0.6
Ge150	Ge−O	3.9 ± 0.3	1.78 ± 0.01	5.4 ± 1.7	3.9 ± 0.6	2.1 ± 0.4
Ge300	Ge−O	3.9 ± 0.4	1.76 ± 0.01	4.9 ± 1.5	3.9 ± 0.4	0.5 ± 0.3
Ge500	Ge−O	4.0 ± 0.4	1.75 ± 0.01	4.9 ± 1.2	4.3 ± 0.5	0.5 ± 0.3
Ge700	Ge−O	4.0 ± 0.4	1.74 ± 0.01	4.6 ± 1.3	4.3 ± 0.4	0.3 ± 0.3
a-GeO_2	Ge−O	3.8 ± 0.5	1.74 ± 0.02	3.0 ± 1.1	4.9 ± 0.6	
q-GeO_2	Ge−O	3.9 ± 0.5	1.74 ± 0.01	3.5 ± 1.1	5.3 ± 0.6	

[a] N, R, σ^2, and ΔE are respectively the coordination number, bond length, Debye−Waller factor, and energy threshold shift. $\sigma^{(3)}$ is the third cumulant.

BSRF. In these temperature-dependent XRD, SAXS, and XAFS experiments, Ge025 powder sample was well-mixed with boron nitride (BN) powder and pressed into a pill-like shape. The jump of Ge K-edge was controlled to approximate to 1.0 by adjusting the content of Ge025, where BN was identified to be stable and can be used as the supporting material for high-temperature measurements. The pill-like sample Ge025 was heated to 150, 300, 500, and 700 °C with a heating rate of 8 °C/min. After half-hour heat-preservation at each target temperature, its EXAFS spectrum was collected and denoted as Ge150, Ge300, Ge500, and Ge700, respectively. The heating temperature was stabilized within ±2 °C. The storage ring was run at 2.2 GeV with an average electron current of 80 mA. Incident X-ray was monochromatized by a water-cooling double-crystal Si (111) monochromator with energy resolution ($\Delta E/E$) of 2×10^{-4}.

EXAFS Data Analysis

The EXAFS data of Ge K-edge were treated by using WinXAS 3.1 package.[22] The energy thresholds were determined from the maxima of the first differential quotient of the absorption spectra. Preedge backgrounds were obtained with linear least-squares fitting and were subtracted. Postedge backgrounds were fitted with cubic spline function. The EXAFS signals were extracted by removing the postedge background and were normalized with the absorption-edge jump. Fourier transform of the EXAFS signals were performed with k^3-weight from 2.2 to 12.5 Å^{-1}. The local EXAFS functions were isolated from the Fourier transform (FT) spectra in the region of 0.72−1.79 Å. Reference amplitude and the phase shift of the Ge−O bond were calculated with FEFF code[23,24] on the basis of the crystalline parameters of quartz-type GeO_2 (marked as q-GeO_2) with space group $P3_12_1$ (ICSD-79643). Due to the transferability of amplitude and phase shifts, the local EXAFS curves can be fitted with the following formula:

$$\chi_j(k) = \frac{N_j S_0^2}{k r_j^2} F_j(k)\, e^{-2r_j/\lambda}\, e^{-2k^2\sigma_j^2} \sin(2kr_j + \varphi_j + \Sigma_j) \quad (1)$$

$$\Sigma_j = -4\frac{k\sigma_j^2}{r_j} - \frac{4}{3}k^3\sigma_j^{(3)} \quad (2)$$

where N_j, r_j, σ_j^2, and $\mathbf{\Delta} E_j$ are respectively coordination number, bond length, Debye−Waller factor, and energy threshold shift of the jth coordination shell. $\sigma_j^{(3)}$ is the third cumulant; λ is the mean electron free path. $F(k)$ is the reference amplitude, and ϕ_j is the reference phase shift. The coordination parameters of the unknown samples were obtained as listed in Table 1. The uncertainties of the fitting results were estimated according to the method proposed in the literature.[25,26]

4. Results and Discussion

It has been confirmed that the cylinder micelles may form at a very low surfactant concentration.[27] CTAB is an amphiphilic surfactant molecule composed of hydrophobic and hydrophilic parts. In aqueous solution above the critical micelle concentration (cmc), CTAB assembles into cylindrical structures that maintain the hydrophilic parts of the surfactant in contact with water while shielding the hydrophobic parts within the micellar interior. A TEM micrograph of sample Ge025 is shown in Figure 1. It can be observed that Ge025 has blanket-like morphology with width from dozens of to hundreds of nanometers and length of several micrometers. The fine hairs shown in Figure 1 imply that CTAB has formed the cylindrical nanostructure. Evidently, it was through the condensation of inorganic germanium oxide onto the surfaces of cylinder micelles; these CTAB cylinder micelles were slowly aggregated to form the blanket-like mesostructure. Figure 2 shows the high-resolution TEM (HRTEM) image of the blanket-like morphological germanium oxide. Alternately dark and bright stripes reveal clearly a long-range-ordered mesostructure with periodic length of about 5.3 nm. To improve the contrast of the HRTEM image, fast Fourier transform (FFT) of Figure 2 was performed and shown as the inset of Figure 2. The dark stripes correspond to the germanium oxide wall, and the bright stripes correspond to the nanotubes of surfactant CTAB. These nanotubes have uniform diameter of about 3.2 nm with several micrometers in length; every hundreds of nanotubes connected with germanium oxide are self-assembled into one blanket.

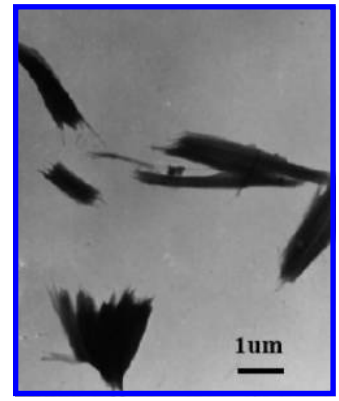

Figure 1. TEM micrograph of the as-prepared germanium oxide sample, which shows a blanketlike morphology. Each blanket consists of hundreds of one-dimensional CTAB nanotubes.

Small-angle XRD was used to determine the mesostructure of the as-prepared sample. Four diffraction peaks were found and can be, respectively, indexed as (002), (003), (004), and (005) reflections, as shown in Figure 3. Because none but these (00l) reflections can be found, it illustrates that the as-prepared sample has self-assembled into one-dimensional long-range-ordered mesostructure. This is obviously different from the cubic or hexagonal mesostructures. Although lamellar mesostructure has also the similar (00l) diffraction pattern, the cylindrical

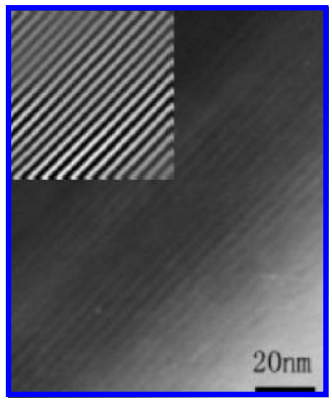

Figure 2. HRTEM image of the as-prepared sample and the corresponding FFT image as shown in the inset. Alternately dark and bright stripes reveal a surfactant-assisted self-assembly mesostructure.

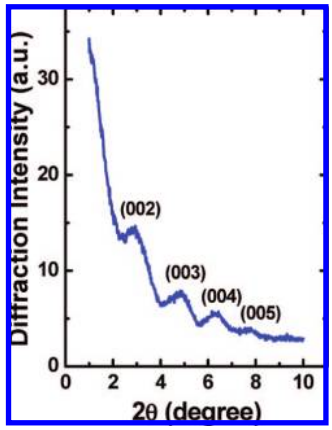

Figure 3. Small-angle XRD pattern of the as-prepared germanium oxide sample. Four diffraction peaks confirms the one-dimensional long-range-ordered mesostructures of germanium oxide.

structure of each CTAB micelle as confirmed by the fine hair in the TEM image demonstrates that a lamellar structure is inconsequential, because the cylinders can only be assembled into blanket-like structure or hexagonal structure. Even if these cylinders can be assembled into some lamellar-like structure, then a two-dimensional long-range-order structure should be presented. However, the X-ray diffraction patterns do not support this lamellar-like structure or hexagonal structure. In addition, the concentration of surfactant CTAB in the sample preparation is not high enough to form a lamellar structure according to the literature.[27] Third, the diffraction peaks as shown in Figure 3 are much broader compared with those of lamellar structures.[1,19,37] Therefore, on the basis of TEM observation and XRD pattern, we think that surfactant CTAB and germanium oxide have assembled into blanket-like mesostructures. Because of the sharp increasing of X-ray scattering intensity with the incident X-ray direction approximating to direct beam, the (001) reflection is not easy to be clearly observed from the XRD pattern. Fortunately, the (001) reflection was confirmed from the SAXS measurements as shown in Figure 4. An average lattice parameter of 5.5 nm can be obtained from all these diffraction peaks. The X-ray result is consistent with the result from TEM. Wide-angle XRD measurements were used to probe the crystalline structures of the germanium oxide; however, no detectable diffraction peaks can be observed in the temperature range from RT to 700 °C. This means that the mesostructured germanium oxide in the blankets always keeps an amorphous form in the given temperature range.

Figure 4a shows the temperature-dependent SAXS curves. It can be found that the low-angle scattering intensity increases with the heating temperature increasing. From the viewpoint of SAXS, there are two possible reasons for the relative increase of low-angle scattering intensity. One is the particle size increasing; another is the increase of the electron-density difference. Because of the unchanged mesostructure below 300 °C, we believe that the increase of low-angle scattering intensity is due to the increase of the electron-density difference, which is because the hydrocarbons from the surfactant CTAB and the adsorptive water were gradually burnt off with the heating temperature increasing. As the heating temperature is higher than 300 °C, the long-range ordered mesostructure has been destroyed and collapses as confirmed by Figure 4b. The germanium oxide has been gradually agglomerated together. In this case, the relative increase of the low-angle scattering intensity can be attributed to the increase of the particle size.

In Figure 4b, a clear shape difference of SAXS curves can be observed. The broadened feature α located at about 1.62° in Ge025 indicates a long-range-ordered structure with a period of about 5.5 nm. This feature can be indexed as the (001) reflection; other higher index reflections were shown in Figure 3. When the sample is heated to 150 °C, the adsorptive water[28] in the sample has been lost. This results in the SAXS intensity increasing. However, the feature α does not change compared with that of Ge025, which means that the adsorptive water does not affect the mesostructure. That is to say, these germanium oxide blankets still keep the similar mesostructures at 150 °C as in room temperature. As the sample was heated to 300 °C, the intensity of feature α increased, as shown in Figure 4b. This is because the surfactant CTAB had been partially decomposed, and its tail chain becomes short. It is in agreement with the previous report[29,30] that surfactant CTAB starts decomposing above 180 °C. At the same time, the structural water in the sample also starts to dehydrate. When the heating temperature was further up to 500 °C, feature α disappears completely, indicating that surfactant CTAB had been completely burnt off. In this case, the long-range-ordered mesostructure have been completely collapsed. From the in-situ heating SAXS results, we can concluded that the loss of adsorptive water does not affect the mesostructure of germanium oxide blankets, whereas the surfactant CTAB plays an important role in keeping this mesostructure of germanium oxide blankets.

The local atomic structures around germanium in this mesostructure were determined by using XAFS technique. Figure 5 shows the change of the normalized Ge K-edge X-ray-absorption near-edge structure (XANES) spectra with heating temperature. The main peak (near $E - E_0 = 0$) corresponds to the electron transition from 1s to 4p. There are two features A and B existing in these XANES spectra. The high-energy features B can be attributed to the multiple scattering inside the first oxygen shell.[31] It can be seen from Figure 5 that features A in l-GeO_2, Ge025, and Ge150 are very similar. With heating temperature increasing, however, feature A become smoother. Especially, as the heating temperature is up to 700 °C, feature A shows a drastic change and is split into two components. This feature in Ge700 is more similar to that in bulk amorphous-GeO_2 (marked as a-GeO_2) as compared in Figure 5, which implies that Ge700 has a similar structure with a-GeO_2. The tendency of bond-length variation can be also evaluated from the XANES features. It was known[32] that the resonance energy E_r and the bond length R of the confining shell are linked by the relation E_rR = constant. Figure 5 shows that features B move toward high energy with the heating temperature increasing,

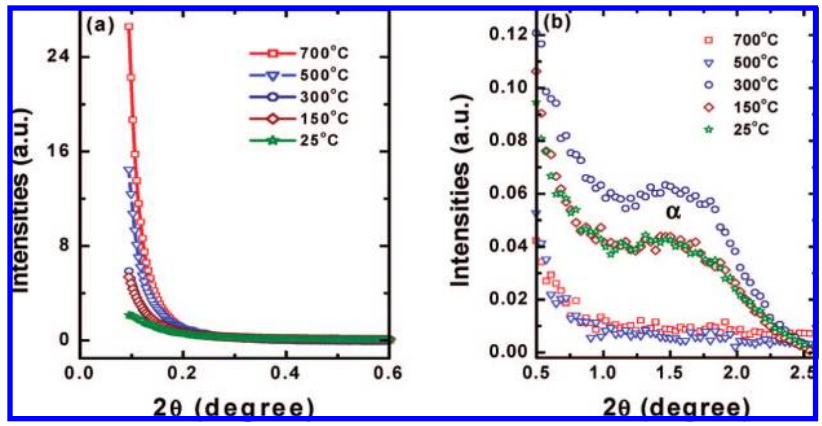

Figure 4. In-situ heating SAXS curves. (a) Scattering angle 2θ from 0.0 to 0.6° (left panel); (b) scattering angle 2θ from 0.5 to 2.5° (right panel). The variation of scattering intensity means the change of electron-density difference. Feature α disappearance implies that the mesostructure was destroyed and surfactant CTAB was completely burnt off.

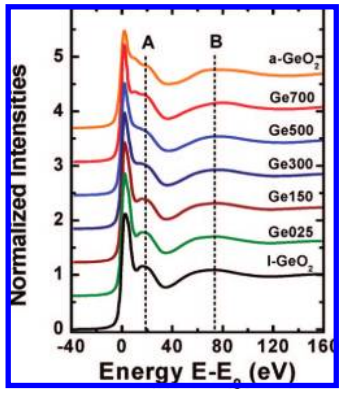

Figure 5. In-situ heating Ge K-edge XANES spectra. Feature A shows the change of local atomic structure, and feature B shows the tendency of Ge−O bond-length contraction with temperature increasing.

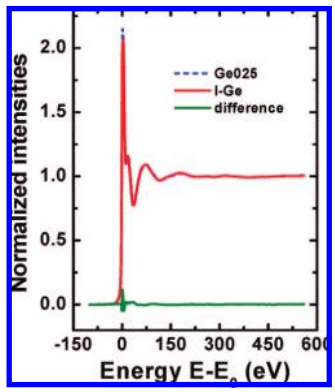

Figure 6. Comparison of Ge K-edge EXAFS spectra between l-GeO_2 and Ge025. Evidently, GeO_2 solution has the same local atomic structure with the as-prepared sample.

implying the first Ge−O bond-length constriction with temperature increasing. The Ge K-edge X-ray-absorption spectra of l-GeO_2 and Ge025 as well as their difference spectrum are shown in Figure 6. It can be found that l-GeO_2 and Ge025 have almost the same EXAFS signals. The slight difference is in their intensities of "white line". Therefore, from the XANES spectra, it can be concluded that l-GeO_2 has the same local atomic structure with the as-prepared sample Ge025. With the heating temperature increasing, the local atomic configuration around Ge is almost maintained until 700 °C, but the Ge−O bond length shows a contraction tendency. At about 700 °C, the local atomic structure around Ge has returned to the structure of a-GeO_2 at room temperature.

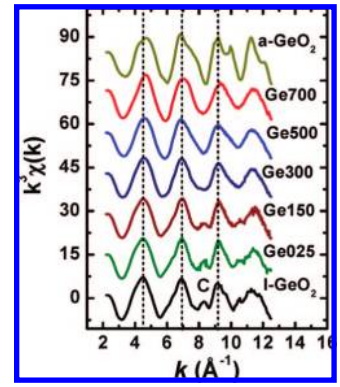

Figure 7. Comparison of Ge K-edge k^3-weighted EXAFS signals. Feature C is from the Ge−O−Ge atom-pair contribution.

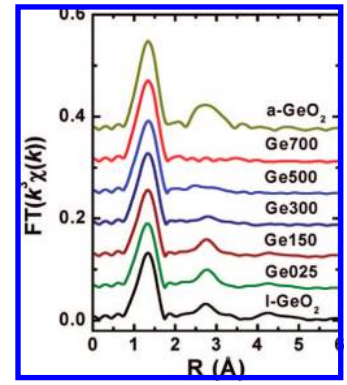

Figure 8. Comparison of Ge K-edge FT spectra with k^3-weight. Ge−O−Ge coordination shell can only be observed below 300 °C.

In-situ heating EXAFS signals of Ge K-edge with k^3-weight are compared in Figure 7. An obvious feature C appears at about 8.3 $Å^{-1}$ on the EXAFS signals of l-GeO_2, Ge025, and Ge150. It can be identified by FEFF calculation that feature C is mainly from the contribution of the second neighbors Ge−O−Ge atom pair. When the heating temperature is higher than 300 °C, feature C disappears, which corresponds to the disappearance or weakening of the Ge−O−Ge coordination as confirmed by the FT spectra shown in Figure 8. Usually with temperature change, there are always two intercompeting factors acting on the local atomic structures of nanomaterials. One is the static order; the other is the thermal disorder. When the rate of rise of static order is bigger than the rate of rise of thermal disorder, the atomic structure of nanomaterials tends to perfection; otherwise, it will become more disordered. By comparing the Ge−O−Ge

coordination peaks located at about 2.75 Å in Figure 8, it can be seen that the structural completeness is almost the same for the samples with temperature lower than 300 °C, but their Ge−O−Ge coordination peaks are very different from a-GeO_2. Although these samples show Ge−O−Ge peaks at the same position as a-GeO_2, the magnitudes of these Ge−O−Ge coordination peaks are weaker. It is well-known that a limited particle size (e.g., a few nanometers) will decrease the average higher shell (e.g., Ge−O−Ge) coordination number if the end atom (e.g., Ge) cannot be supplied from the circumambience. Evidently, the Ge−O−Ge coordination number is lower in these samples below 300 °C than in the bulk a-GeO_2. However, the Ge−O−Ge coordination peak suddenly becomes more disordered, even disappears around 300 °C. Because the temperature is higher than 300 °C, only the Ge−O coordination can be observed. The disappearance of the Ge−O−Ge peak corresponds to the complete decomposition of surfactant CTAB. But the decomposition of CTAB seems to be not enough to destroy completely the Ge−O−Ge coordination and there should be still Ge−O−Ge bonds in the wall. Actually, the disappearance of Ge−O−Ge peaks is relative to the evaporation of the structural water in germanium oxide, which will cause larger structural disorder. It was the smaller particle size and the larger thermal and structural disorders that make the Ge−O−Ge shell invisible on the FT spectra. This will be further discussed later. Another interesting phenomenon is that the Ge−O coordination peak shows an opposite thermal behavior with the Ge−O−Ge coordination peak as the temperature increase. That is to say, the decomposition of CTAB and the evaporation of the structural water do not damage the structures of the Ge−O coordination; even the Ge−O shell benefits from them. As shown in Figure 8, even for the amorphous GeO_2, the Ge−O−Ge coordination is still visible. Therefore, when the surfactant CTAB is completely burnt off and the structural water is evaporated, the material cannot keep the same mesostructure and the particle size of nanostructured germanium oxide should be grown, but the medium- or long-range order is decreased because the second coordination peak that came from the Ge−O−Ge atom pairs is disappearing instead of strengthening. All these clearly tell us that CTAB is a supporting frame to maintain the germanium oxide mesostructure. After the decomposition of the surfactant CTAB, the aggregation of germanium oxide within the measurement temperature range does not make the medium-range and long-range structures more ordered because of the evaporation of structural water. But, due to the collapse of the CTAB frame as well as the substitution of oxygen for hydroxyl, partial structural strain can be released which results in more order of the Ge−O coordination shell. However, the heating temperature is not enough to make the sample transforming to crystalline structure from the amorphous phase. That is why we cannot observe the crystalline diffraction peaks in the whole measurement temperature range.

We note surprisingly that a Ge−O−Ge coordination shell exists also in GeO_2 solution as shown on the FT spectrum of l-GeO_2. It was reported[33,34] that l-GeO_2 has two dominant components $Ge(OH)_4^0$ and $GeO(OH)_3^-$ in alkaline solutions, in which Ge atoms are all coordinated with four oxygen atoms. The appearance of the high coordination shell (Ge−O−Ge) proves that germanium atoms not only exist in the two molecules in the GeO_2 alkaline solution (l-GeO_2) but also some polymerization of $Ge(OH)_4^0$ and $GeO(OH)_3^-$ molecules occurs. A possible polymerization mode is shown in Figure 9. Because the polymerization degree is not so high, the average Ge−O−Ge coordination number is quite low. Therefore, only a weak

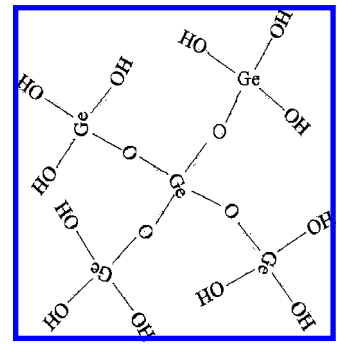

Figure 9. A possible polymerization mode of $Ge(OH)_4^0$ and $GeO(OH)_3^-$ in GeO_2 alkaline solution.

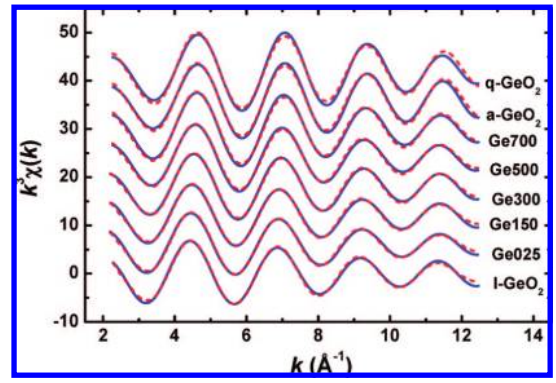

Figure 10. Comparison of Ge K-edge EXAFS signals with k^3-weight between the experimental data (solid line) and the best fitting curves (dashed line).

Ge−O−Ge coordination peak can be found from the FT spectrum of the Ge K-edge for l-GeO_2, as shown in Figure 8. That samples Ge025 and Ge150 have the same Ge−O−Ge coordination implies that the same local atomic structures around Ge in l-GeO_2 were maintained in the solid sample Ge025. In other words, there are some hydroxyls (or structural water) coordinated to the germanium atoms except the oxygen atoms. As the sample is heated above 150 °C, although germanium still has four coordinators, the structural water in the sample will be gradually lost. The following reaction probably occurs:

$$Ge(OH)_4^0 + GeO(OH)_3^- \xrightarrow{\Delta} GeO_2 + H_2O\uparrow \qquad (3)$$

In this case, the hydroxyls coordinated to Ge atom have been displaced by oxygen. This substitution process will break down the Ge−O−Ge coordination and cause Ge−O−Ge disorder increase. It was the substitution of oxygen for hydroxyl or the evaporation of structural water that results in the Ge−O−Ge coordination disappearance. This will be further confirmed by the EXAFS fitting. Although EXAFS technique cannot distinguish directly the backscatters between hydroxyl and oxygen, the obtained Ge−O bond length is still helpful to judge the backscatters.

From the FT spectra of the Ge−K edge EXAFS curves as shown in Figure 8, the Ge−O coordination shells were isolated to get the first near-neighbor EXAFS functions surrounding Ge centers as shown in Figure 10. A symmetrical Gaussian function was tested to fit the experimental data, but no reasonable fitting parameters can be obtained. Therefore, a slightly asymmetrical atom-pair distribution model with the $\delta^{(3)}$ cumulant was introduced to fit the Ge−O coordination distribution. The best fitting structural parameters are listed in Table 1. The corre-

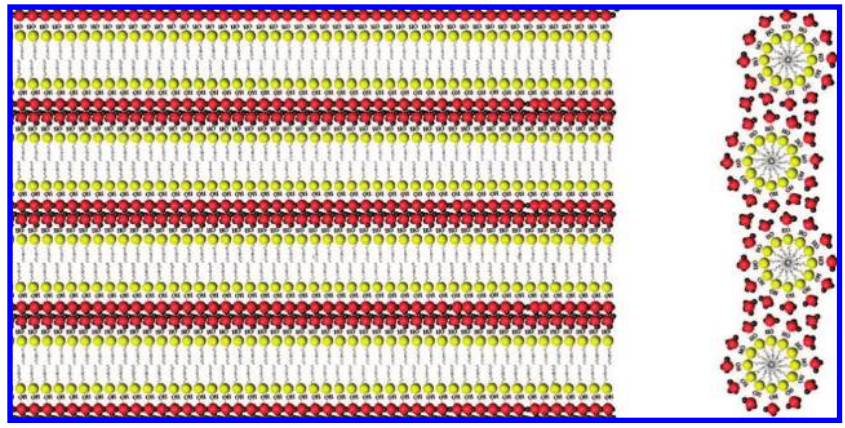

Figure 11. Setch map of the mesostructured germanium oxide.

sponding fitting curves are also shown in Figure 10. It was reported[28] that the adsorptive water can be removed from a sample below 150 °C. However, Ge025 and Ge150 were fitted to have almost the same structural parameters. Therefore, the adsorptive water has no obvious effect on the local atomic structures of the mesostructured germanium oxide. This is well-consistent with SAXS analysis. By comparing the structural parameters, it can be found that GeO_2 (l-GeO_2) solution and the as-prepared sample Ge025 have very similar Ge−O coordination except a 0.01 Å change of Ge−O bond length. This confirms again that the as-prepared sample Ge025 inherits the local atomic structures from the GeO_2 solution.

From Table 1, it can be found that the Ge−O coordination number is always 4 for the sample heated at different temperatures. However, the Ge−O bond length shortens from 1.79 to 1.74 Å as the heating temperature rises from RT to 700 °C. This change of Ge−O bond length is in good agreement with the XANES analysis, but it is obviously ambivalent with the common thermal expansion rule. This is because the evaporation of structural water makes hydroxyl gradually be substituted by oxygen. Evidently, the Ge−OH coordination bond length is larger than the Ge−O coordination bond length due to the larger spatial steric hindrance of hydroxyl than oxygen. Although hydroxyl and oxygen backscatters cannot be directly distinguished, the Ge−O bond-length change can be well-explained by the substitution of backscatters. In addition, this contraction of the Ge−O bond length can be partially attributed to the supporting-frame collapse of the cationic surfactant CTAB. In the sample preparation, Ge^{4+} ions cannot exist in the solution, and a cationic group cannot also be directly attracted to the surface of surfactant CTAB, because the hydrophilic head (CTA^+) of CTAB is outward. In alkaline solutions, two dominant components $Ge(OH)_4^0$ and $GeO(OH)_3^-$ are attracted to the surface of CTAB through hydroxyl forming the $Ge^{4+}-OH^--CTA^+$ bridge bonds. With the temperature increasing, surfactant CTAB was partially or completely decomposed. As the sample was heated higher than 300 °C, CTAB was burnt off and the bonding of $Ge^{4+}-OH^--CTA^+$ was broken up until disappearing. In this case, the restriction of the supporting frame to germanium oxide and the tensile stress acting on germanium oxide was released. Therefore, the Ge−O bond length was gradually restored to the equilibrium bond length, i.e., the Ge−O bond length in crystalline q-GeO_2 or bulk a-GeO_2. a-GeO_2 is expected to have a local atomic structure similar to q-GeO_2.[35] In this study, a-GeO_2 has been identified to have four oxygen backscatters around Ge with a Ge−O distance of 1.74 Å, which is well-consistent with the previous report.[36] The fitting results identify that Ge700 has the same Ge−O coordination structures with a-GeO_2. Simultaneously, it demonstrates that the structural water has been completely evaporated at 700 °C.

Huo and his co-workers proposed four synthesis routines with (S^+I^-), (S^-I^+), ($S^+X^-I^+$), and ($S^-M^+I^-$) direct and mediated combinations of surfactant (cationic S^+, anionic S^-) and soluble inorganic (cationic I^+, anionic I^-) molecular species for the formation of organic−inorganic mesostructure.[19,37] Wang et al.[28] used the $S^+X^-I^+$ assembly pathway synthesizing mesostructured tin oxide under acidic conditions at room temperature. In this study, mesostructured germanium oxide was prepared under alkaline conditions at 100 °C; the $S^+X^-I^+$ assembly pathway can be also used to explain the formation mechanism of mesostructured germanium oxide. According to the synthetic procedure, the surfactant templating agent CTA^+ (S^+) was preferentially self-assembled with the intermediate anion OH^- (X^-) to form a buffer layer, which can compensate the repulsion between the CTA^+ and Ge^{4+} in $Ge(OH)_4^0$ and $GeO(OH)_3^-$ molecules. Both dominant components $Ge(OH)_4^0$ and $GeO(OH)_3^-$ in solution are gradually condensed onto the surface of the CTAB cylindrical micelle. Finally, partial CTAB micelles coated by germanium oxide are aggregated together to form the mesostructure. A sketch map of the mesostructured germanium oxide is shown in Figure 11. From the SAXS (Figure 4b) and EXAFS (Figure 7 and Figure 8) measurements, we know that this mesostructured GeO_2 is stable below 300 °C.

5. Conclusion

By using a surfactant-templated approach, mesostructured germanium oxide has been successfully synthesized under basic hydrothermal conditions. TEM observation and in-situ heating XRD, SAXS, and XAFS techniques were used to investigate the structural change of this germanium oxide mesostructure with heating temperature. The as-prepared sample was identified to have a blanket-like configuration; each blanket consists of hundreds of one-dimensional nanotubes. The surfactant CTAB plays a support role for keeping this mesostructure, which is stable below 300 °C. The as-prepared sample Ge025 inherits the local atomic structures around Ge from the GeO_2 alkaline solution. The adsorptive water has no effect on the mesostructures and the local atomic structures. With the temperature increasing, the local atomic structures around Ge change slightly with the surfactant CTAB decomposition and the evaporation of structural water. The Ge−O bond length presents a negative thermal expansion behavior and correlates with the substitution of oxygen for hydroxyl. After decomposition of CTAB, the mesostructure can be completely destroyed. The complete substitution

of oxygen for hydroxyl makes the Ge−O−Ge coordination disappear and the Ge−O bond length return to the value in quartz-GeO_2. Germanium oxide always keeps an amorphous status, and the local atomic structures are quite similar with a-GeO_2 as the temperature is up to 700 °C. Germanium atom is always coordinated with four oxygen atoms in the measurement temperature range. The formation mechanism of this mesostructured germanium oxide has been proposed.

Acknowledgment. This work is supported by the National Natural Science Foundation of China with Grant No. 10374087, the Knowledge Innovation Program of the Chinese Academy of Sciences (Grant Nos. KJCX3-SYW-N8 and KJCX2-SW-N11), the Outstanding Youth Fund (Grant No. 10125523), and the Key Important Nano-Research Project (Grant No. 90206032) of the National Natural Science Foundation of China.

References and Notes

(1) Beck, J. S.; Vartuli, J. C.; Roth, W. J.; Leonowicsw, M. E.; Kresge, C. T.; Schmitt, K. D.; Chu, C. T. W.; Olson, D. H.; Sheppard, E. W.; McCullen, S. B.; Hinggins, J. B.; Schlenker, J. L. *J. Am. Chem. Soc.* **1992**, *114*, 10834.

(2) Yuan, Z.; Zhou, W. *Chem. Phys. Lett.* **2001**, *33*, 427.

(3) Zhao, D.; Feng, J.; Huo, Q.; Melosh, N.; Fredirckson, G. H.; Chemlka, B. F.; Stucky, G. D. *Science* **1998**, *279*, 548.

(4) Lin, H. P.; Mou, C. Y.; Liu, S. B. *Adv. Mater.* **2000**, *12*, 103.

(5) Lange, T.; Njoroge, W.; Wewas, H.; Beckers, M.; Wuttig, M. *Thin Solid Film* **2000**, *365*, 82.

(6) Bai, Z. G.; Yu, D. P.; Zhang, H. Z.; Ding, Y.; Wang, Y. P.; Gai, X. Z.; Hang, Q. L.; Xiong, G. C.; Feng, S. Q. *Chem. Phys. Lett.* **1999**, *303*, 311.

(7) Zhang, Y.; Zhu, J.; Zhang, Q.; Yan, Y.; Wang, N.; Zhang, X. *Chem. Phys. Lett.* **2000**, *217*, 504.

(8) Wu, X. C.; Song, W. H.; Zhao, B.; Sun, Y. P.; Du, J. J. *Chem. Phys. Lett.* **2001**, *349*, 210.

(9) Zacharias, M.; Fauchet, P. M. *J. Non-Cryst. Solids* **1998**, *227*, 1058.

(10) Maeda, Y. *Phys. Rev. B* **1995**, *51*, 1658.

(11) Lu, Q. Y.; Gao, F.; Li, Y. Q.; Zhou, Y. M.; Zhao, D. Y. *Microporous Mesoporous Mater.* **2002**, *56*, 219.

(12) Murray, S.; Trudeau, M.; Antonelli, D. M. *Adv. Mater.* **2000**, *12*, 1339.

(13) Cabrera, S.; Haskouri, J. E.; Alamo, J.; Beltrán, A.; Beltrán, D.; Mendioroz, S.; Marcos, M. D.; Amorós, P. *Adv. Mater.* **1999**, *11*, 379.

(14) Qi, L.; Ma, J.; Cheng, H.; Zhao, Z. *Langmuir* **1998**, *14*, 2579.

(15) Severin, K. G.; Abdel-Fattah, T. M.; Pinnavaia, T. J. *Chem. Commun. (Cambridge)* **1998**, *14*, 1471.

(16) Beck, J. S.; Vartuli, J. C.; Roth, W. J.; Leonouries, M. E.; Kresege, C. T.; Schmitt, K. D.; Chu, C. T. W.; Dson, D. H.; Sheppard, E. W.; McCullen, S. B.; Higgins, J. B.; Schlenke, J. L. *J. Am. Chem. Soc.* **1992**, *114*, 10834.

(17) Monnier, A.; Schuth, F.; Huo, Q.; Kumar, D.; Margolese, D.; Maxwell, R. S.; Stucky, G. D.; Krishnamurty, M.; Petroff, P.; Firouzi, A.; Janicke, M.; Chmelka, B. F. *Science* **1993**, *261*, 1299.

(18) Firouzi, A.; Kumar, D.; Bull, L. M.; Besier, T.; Sieger, P.; Huo, Q.; Walker, S. A.; Zasadzinski, J. A.; Glinka, J. A.; Nicol, J.; Margolese, D.; Stucky, G. D.; Chmelka, B. F. *Science* **1995**, *267*, 1138.

(19) Huo, Q.; Margolese, D. I.; Ciesla, U.; Feng, P.; Gier, T. E.; Sieger, P.; Leon, R.; Petroff, P. M.; Schuth, F.; Stuchy, G. D. *Chem. Mater.* **1994**, *6*, 1176.

(20) Dong, B. Z.; Sheng, W. J.; Yang, H. L. *J. Appl. Crystallogr.* **1997**, *30*, 877.

(21) Chen, Z. J.; Wu, Z. H.; Sun, M. H.; Chen, X.; Cai, Q.; Yang, S. S. *High Energy Phys. Nucl. Phys.* **2005**, *29*, 321.

(22) Ressler, T. *J. Synchrotron Radiat.* **1998**, *5*, 118.

(23) Ankudinov, A. L.; Ravel, B.; Rehr, J. J.; Conradson, S. D. *Phys. Rev. B* **1998**, *58*, 7565.

(24) Ankudinov, A. L.; Bouldin, C.; Rehr, J. J.; Sims, J.; Hung, H. *Phys. Rev. B* **2002**, *65*, 104107.

(25) Li, G. G.; Bridges, F.; Brooth, C. H. *Phys. Rev. B* **1995**, *52*, 6332.

(26) Joyner, R. W.; Martin, K. J.; Meehan, P. *J. Phys. C* **1987**, *20*, 4005.

(27) Brinker, C. J.; Lu, Y.; Sellinger, A.; Fan, H. *Adv. Mater.* **1999**, *11*, 579.

(28) Wang, Y. D.; Ma, C. L.; Sun, X. D.; Li, H. D. *Inorg. Chem. Commun* **2001**, *4*, 223.

(29) Wang, Y. D.; Ma, C. L.; Sun, X. D.; et al. *Microporous Mesoporous Mater.* **2001**, *49*, 171.

(30) Gao, Q.; Chen, J.; Xu, R. *Chem. Mater.* **1997**, *9*, 457.

(31) Wu, Z. Y.; Jollet, F.; Seifert, F. *J. Phys.: Condens. Matter* **1998**, *10*, 8083.

(32) Natoli, C. R. I *EXAFS and Near Edge Structure*; Bianconi, A.,Incoccia, L., Stipcich, S.; Springer Series in Chemistry and Physics; Springer: Berlin, 1983; pp 43.

(33) Pokrovski, G. S.; Schott, J. *Geochim. Cosmochim. Acta* **1998**, *62*, 1631.

(34) Pokrovski, S.; Martin, F.; Hazemann, J. L.; Schott, J. *Chem. Geol.* **2000**, *163*, 151.

(35) Itie, J. P.; Polian, A.; Calas, G.; Petiau, J.; Fontanine, A.; Tolentino, H. *Phys. Rev. Lett.* **1989**, *63*, 398.

(36) David, L. P.; Saboungi, M. L. *Phys. Rev. Lett.* **1998**, *81*, 3207.

(37) Huo, Q.; Margolese, D. I.; Ciesla, U.; Feng, P.; Gier, T. E.; Sieger, P.; Leon, R.; Petroff, P. M.; Schuth, F.; Stuchy, G. D. *Nature* **1994**, *368*, 317.

JP803407A